Muon Scattering and Dimuon Production

E. Gabathuler, CERN
Session Organizer

THE EMC MUON SCATTERING EXPERIMENT AT CERN

Hans-Erhart Stier
University of Freiburg
D-7800 Freiburg, Germany

European Muon Collaboration: O.C. Allkofer[4], J.J. Aubert[6], G. Bassompierre[6], K.H. Becks[12], Y. Bertsch[6], C. Best[1], E. Böhm[4], D.R. Botterill[9], F.W. Brasse[2], C. Broll[6], J. Carr[9], R.W. Clifft[9], J.H. Cobb[5], G. Coignet[6], F. Combley[10], G.R. Court[7], J.M. Crespo[6], P. Dalpiaz[11], P.F. Dalpiaz[11], W.D. Dau[4], J.K. Davies[8], Y. Declais[6], R.W. Dobinson[1], J. Drees[12], A. Edwards[7], M. Edwards[9], J. Favier[6], M.I. Ferrero[11], W. Flauger[2], E. Gabathuler[1], R. Gamet[7], J. Gayler[2], C. Gössling[2], P. Gregory[1], J. Haas[3], U. Hahn[3], P. Hayman[7], M. Henckes[12], J.R. Holt[7], H. Jokisch[4], V. Korbel[2], U. Landgraf[3], M. Leenen[1], L. Massonnet[6], W. Mohr[3], H.E. Montgomery[1], K. Moser[3], R.P.Mount[8], P.R.Norton[9], A.M. Osborne[1], P. Payre[1], C. Peroni[11], H. Pessard[6], K. Rith[1], M.D. Rousseau[9], E. Schlösser[3], M. Schneegans[6], T. Sloan[5], M. Sproston[9], H.E. Stier[3], W. Stockhausen[12], J.M. Thénard[6], J.C. Thompson[9], L. Urban[6], G. von Holtey[1], H. Wahlen[1], V.A. White[1], D. Williams[7], W.S.C. Williams[8], S.J. Wimpenny[10].

CERN[1]-DESY(Hamburg)[2]-Freiburg[3]- Kiel[4]- Lancaster[5]-LAPP(Annecy)[6]- Liverpool[7]- Oxford[8]- Rutherford[9]- Sheffield[10]- Turin[11] and Wuppertal[12].

1.) Introduction

The investigation of the hadronic structure of the nucleon is one of the most interesting questions in high energy physics. Over the last two decades the electron has proved to be a useful probe of the nucleon structure down to a distance determined by the maximum beam energies available in these years. The increased energy of the proton synchrotrons at FNAL and CERN allowed the production of very high energy lepton beams up to about 300 GeV to overcome the lack of electron accelerators in the multi-hundred-GeV range.

At these high energies the muon becomes a very effective probe of the inner structure of the nucleon at small distances. Quantum electrodynamics allows exact calculation of the electromagnetic interaction vertex of the muon. As shown in fig. 1 the muon is used as a source of virtual photons which probe the hadronic structure of the target nucleon.

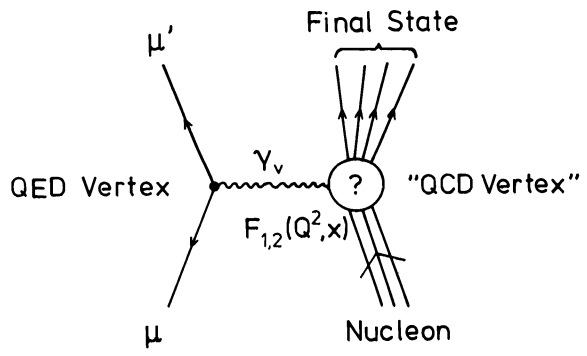

Fig. 1 Diagram for inelastic muon nucleon scattering described by the exchange of a single virtual photon.

The incident and scattered muon energies E and E' plus the scattering angle θ fix the kinematic properties of the virtual photon[1], its energy ν:

$$\nu = E - E'$$

and its imaginary mass squared Q^2:

$$Q^2 = -4EE'\sin^2 \theta/2$$

Early electron scattering experiments [2] have shown the importance of the variable

$$x = \frac{Q^2}{2M\nu}$$

where M is the proton mass, for the description of deep inelastic scattering by two structure functions $F_{1,2}(Q^2,x)$[3].

The Feynman diagram of fig. 1 suggests a description of the photon nucleon vertex by quantum chromodynamics in a way very similar to the well understood QED vertex of virtual photon production by the scattered muon. The naive quark parton model[4] treats the photon nucleon interaction as the interaction of the photon with a single quasifree parton inside the nucleon. The variable x has a physical interpretation in this simple model: it represents the fractional momentum of the struck parton inside the target nucleon at the time of the interaction

$$x \simeq p_{parton}/p_{target}$$

This is reasonable at high energies if transverse parton momenta and mass effects are negligible. If $q_i(x)$ is the probability distribution function for the ith parton inside the target and e_i its charge then the above mentioned structure function F_2 has a simple physical meaning:

$$F_2(x) = \sum_i e_i^2 x q_i(x)$$

It depends on x only and not on Q^2. This interpretation of F_2 explained the initial observation of scaling of the structure function[5] i.e. its approximate independence

of Q^2 which seemed to confirm Bjorken's earlier conjecture[6] of scaling.

The first high energy muon experiments at FNAL[7] as well as electron scattering experiments at SLAC[8] in the lower Q^2 region have shown that scaling is violated. The resolving power of the current probe was improved by increasing Q^2. As predicted by field theories of coloured quarks and gluons, gluon exchange and gluon radiation included in a quark parton model produce a scaling violation[9]. QCD predicts its Q^2 dependence[10]. The $q\bar{q}$ sea is produced by gluons radiated from the valence quarks. Only for $Q^2 \to \infty$ the quarks become asymptotically free.

At finite Q^2 the quarks are not free. Experiments in this region shall see a scaling violation due to gluon exchange. At very high Q^2 and in the high x region scaling should be violated by gluon radiation in analogy to photon radiation by accelerated charges in quantum electrodynamics. At small x, as Q^2 increases, $F_2(x,Q^2)$ should increase, at large x it should decrease[11-13].

The experimental determination of the exact form of scale breaking is thus premature. The data can be used as input to phenomenological quark gluon models to determine the form of sea quark and valence quark momentum distributions inside the nucleon, an important question in modern elementary particle physics.

2.) Muon Beam and EMC Spectrometer

To determine the exact form of the scaling violation a high energy muon beam with an increased intensity compared to earlier muon beams has been set up at the CERN-SPS by the European Muon Collaboration[14]. Fig. 2 shows a schematic view of this beam. The 400 GeV external proton beam of the SPS hits a beryllium target producing a high pion and kaon flux. Pions and kaons are separated from the primary proton beam by a bending magnet due to their lower momenta. The proton beam is then dumped.

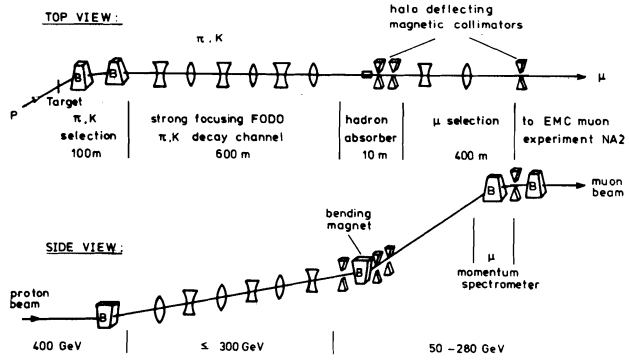

Fig. 2 Schematic view of the CERN muon beam.

Pions and kaons enter a 600 m long strong focussing decay channel. Its magnetic focussing elements can be operated up to momenta of 300 GeV/c. The oscillation of the hadrons in this decay channel increases the probability of muons from π or K decays to be emitted in forward direction. The use of a strong focussing decay channel essentially improves the muon beam intensity.

10m of Beryllium are used to absorb the remaining hadrons at the end ot the decay channel. At the highest beam momenta another 2.4 m of polyethylene are added to the absorber.

Special care is taken to get rid of halo muons very near to the final beam. 7 magnetic collimators deflect these particles away from the beam. At the experiment the ratio of halo muons to beam muons is ~6 %. The layout of the muon beam has been extensively studied by Monte Carlo calculations giving the same result for the muon halo to beam ratio as finally measured.

A spectrometer in the beam line, consisting of several bending magnets and four scintillation counter hodoscope planes, measures the muon momenta with an accuracy $\Delta p/p \simeq 0.4$ %. This measurement improves the knowledge of the incoming particles kinematics. The momentum band accepted by the muon beam is ±5%. The beam momentum distribution measured in the beam momentum station is given in fig. 3 for the case of a 280 GeV/c muon beam with a 300 GeV/c parent particle momentum setting.

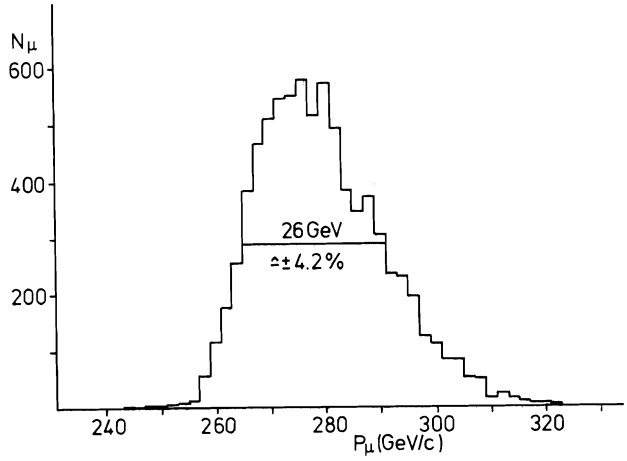

Fig. 3 Beam momentum distribution as measured for a 280 GeV muon beam.

As can be seen from the figure the incoming muon momenta extend between 250 and 320 GeV/c, but they are known with an accuracy of 2 GeV/c. The slight asymmetry in this distribution is as expected from Monte Carlo calculations of pion and kaon decays in the beamline.

The end of the muon beam consists of bending magnets bending the beam coming from 70m under the surface again downwards into the horizontal direction before it enters into the experiment. Typical horizontal and vertical beam distributions at the entrance of the experimental apparatus are shown in fig. 4. Beam intensities vary between 10^7 and 10^8 muons/sec. according to the different beam momenta.

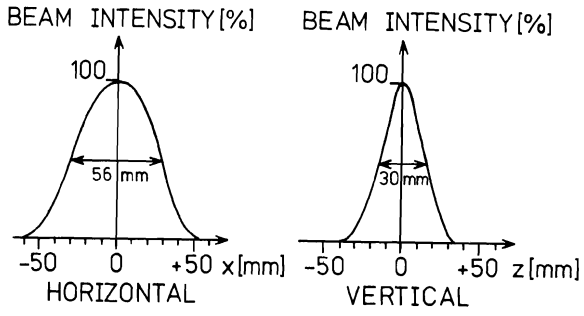

Fig. 4 Typical horizontal and vertical beam distributions.

Fig. 5 shows a top view of the layout of the EMC forward spectrometer. Veto counters V1, V2 and V3 shield the apparatus against halo particle triggers and define the beam size accepted in the experiment by a variable central hole. Further scintillation counter hodoscopes, HBA and HBB, 360 small scintillation counters in total, determine position and angle of the incoming muon if an interaction is registered in the spectrometer.

Different targets have been used in the setup. Data have been taken with a 6m long H_2 and D_2 target cell and also with an iron scintillator sandwich target (STAC target) which increases the luminosity and gives additional information about the total energy deposited in the target in muon scattering events.

The scattered muons are detected in a series of drift chambers, W1-W7 upstream and downstream of the 5.2 Tm spectrometer magnet, the gap of which is filled with a set of proportional chambers P1-P3. All these chambers are deadened in the beam area to be able to stand intensities of the throughgoing beam up to about 10^8 muons/sec. These dead areas are covered by small circular proportional chambers P0a and P0b, 6 planes each, constructed to stand the available beam intensities. The P0 chambers are used to measure muons scattered at very small angles or newly produced particles staying inside or close to the beam area.

The event trigger is produced by different planes of scintillation counter hodoscopes H1-H4. Coincidences of hodoscopes counters are determined by computer programmable matrices[15]. The matrices accept only counter combinations in subsequent hodoscopes pointing to the target region, indicating a variable minimum momentum or a variable minimum scattering angle. These matrix settings have been necessary to reduce the trigger rates to an acceptable level.

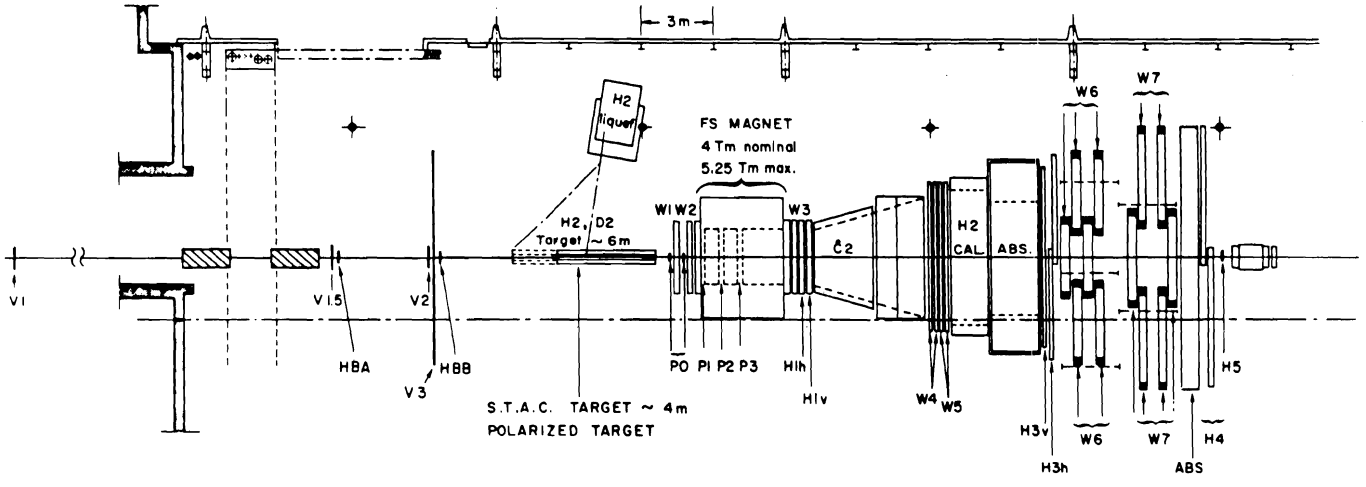

Fig. 5. Schematic layout of the muon scattering experiment as seen from the top.

Hadrons produced in inelastic muon nucleon scattering can be mass selected in a limited momentum range with the aid of a gas Cerenkov counter C2. The scintillation counter hodoscope H2 is built up in the form of a hadron calorimeter to provide some information on hadron energy deposit and to detect neutral particles. All the hadrons are absorbed in a 2 m long hadron absorber consisting of magnetised iron with a small beam hole in the center. The only particles emerging from this magnetized iron block are muons.

The measured data are collected in the apparatus by a CAMAC system read out with the aid of two PDP 11/70 computers. Two other PDP 11/70 computers are mainly used to check the apparatus performance periodically. More details on the electronics, the on line data treatment and the off line data analysis are contained in other preliminary reports given by the collaboration[16-18].

Fig. 6 shows an artist's view of the spectrometer.

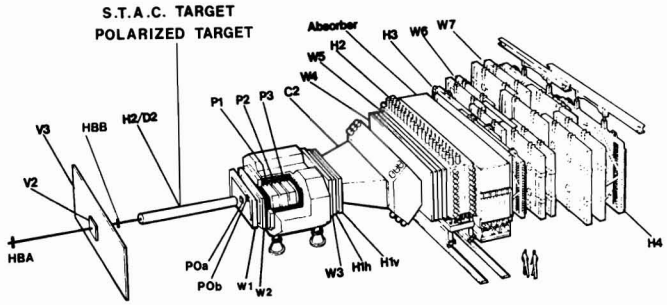

Fig. 6 - Artist's view of the EMC experiment.

3.) Hydrogen Data

3.a. Structure functions.

Since September 1978 data on μp scattering in a hydrogen target have been taken at different beam energies. At energies of 120, 200 and 240 GeV, data corresponding to ≈ 5 x 10^{11} incident muons per energy, have been taken. At 280 GeV beam energy, μp and μn scattering has been investigated by measuring muon nucleon scattering on hydrogen and deuterium targets with about 10^{12} positive muons entering the target in each case.

The off line data analysis has started. Only about 10% of the hydrogen data collected at 280 GeV are presented to this conference. Before the start of the real data production the performance of the experimental apparatus and the off line analysis program chain is being tested with this subset of the data. Nevertheless the statistics of this subset corresponds to the statistics of all high energy muon hydrogen scattering data taken so far outside CERN.

The acceptance of the spectrometer including the cuts introduced in the off line analysis is indicated in fig.7. In the main region of the Q^2-ν plot the acceptance is high (> 70 %) and changes are slow.

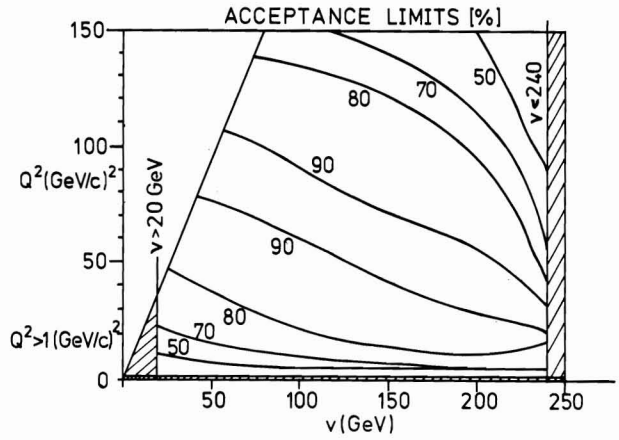

Fig. 7 Lines of constant acceptance in the Q^2-ν plane. The cuts on ν and Q^2 applied to the data are indicated in the figure.

The limitation of ν between 20 and 240 GeV is preliminary and will probably be further reduced with the progress of the data analysis. The high acceptance implies, the off line correction to the raw data is small, the flatness of the acceptance distribution prevents strong changes by the acceptance correction in the Q^2-ν distributions.

Fig. 8 shows the first preliminary results of the dependence of the proton structure function $F_2(x,Q^2)$ on x in the Q^2 range between 8 and 15 $(GeV/c)^2$.

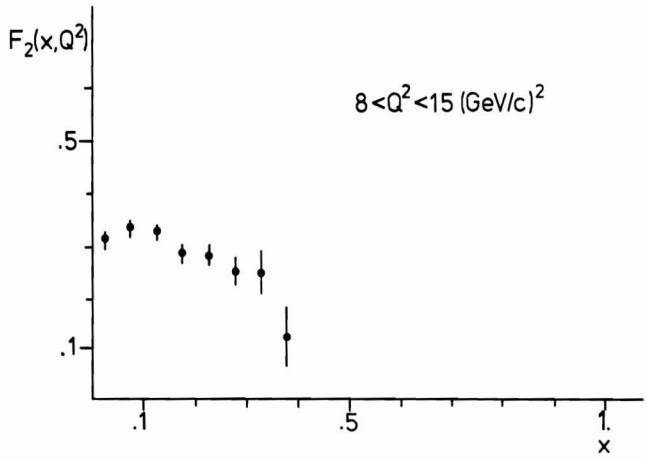

Fig. 8 The structure function $F_2(Q^2,x)$ in the lower Q^2 region.

The data in fig. 9 for the Q^2 range between 15 and 30 $(GeV/c)^2$ are compared to predictions of a QCD calculation by Buras and Gaemers[19]. The data cover a large range of x and can be used to check the assumptions in these model calculations of the x distributions of valence and sea quarks.

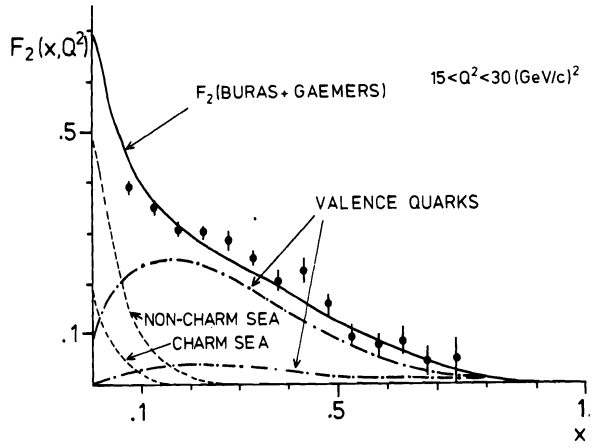

Fig. 9 - Comparison of the data with QCD calculations on the contributions of the different quark types inside the nucleon to the structure function.

Fig. 10a and 10b show the behaviour of $F_2(x,Q^2)$ for high values of Q^2.

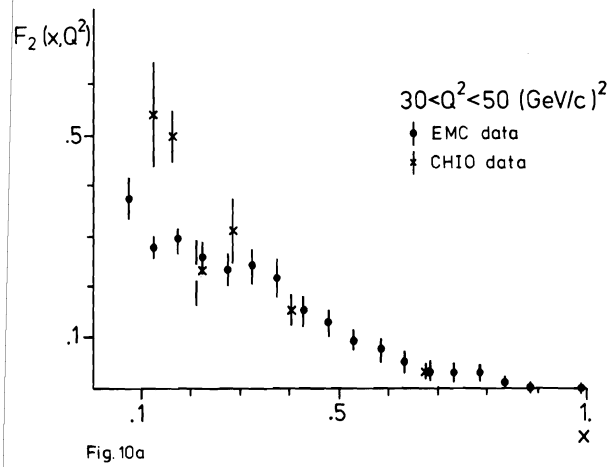

Fig. 10a

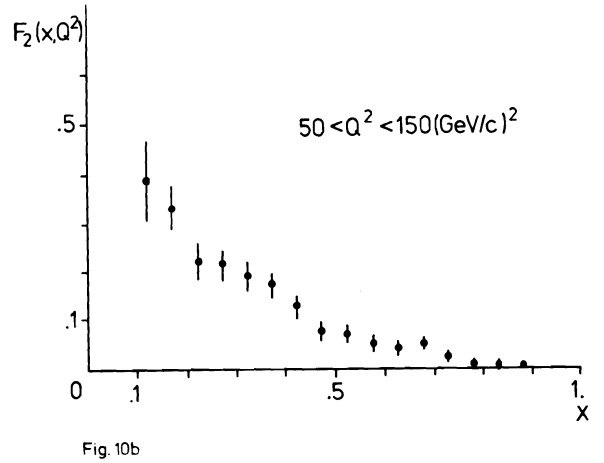

Fig. 10b

Figs. 10a and 10b - $F_2(x,Q^2)$ as measured in this experiment for higher ranges of Q^2 in comparison with the data available from the CHIO collaboration at Fermilab.

Fig. 11 shows the same data in a slightly different representation. The dependence of F_2 on Q^2 is given for various intervals of the scaling variable x. The errors bars shown are statistical errors only. An additional normalisation error of ± 10% has to be added to the data shown in the figure.

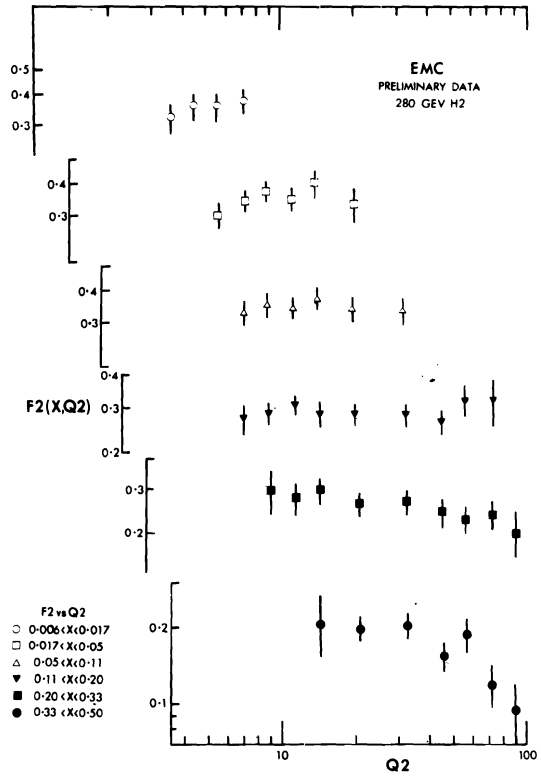

Fig. 11 The structure function dependence on Q^2 for different ranges of x as measured with 280 GeV muons on a hydrogen target.

The general behaviour of the structure function does not show a strong Q^2 dependence, i.e. scaling violation, ever if a slow increase of F_2 with Q^2 at low values and a small decrease of F_2 with Q^2 in the high x region might be visible in this preliminary data set. The improvement in statistics expected from the near future data analysis will be essential to determine the structure functions and the exact form of the scaling violation.

3.b. Hadronic Final States

Muon Scattering experiments on liquid hydrogen targets offer the possibility of studying the hadrons produced in inelastic scattering processes. Since fractionally charged quarks seem to be confined inside the nucleon the outgoing hadrons must reflect final state interactions dressing the struck quark and the remaining diquark system.

A characteristic variable in the study of final states is the hadron momentum p_T transverse to the virtual photon direction. Fig. 12 shows the dependence of $\langle p_T \rangle$ the mean value of p_T, on the ratio z of the total hadronic energy E_H to the virtual photon energy ν:

$$z = \frac{E_H}{\nu}$$

The well known seagul effect, a dip at small values of z, is clearly visible.

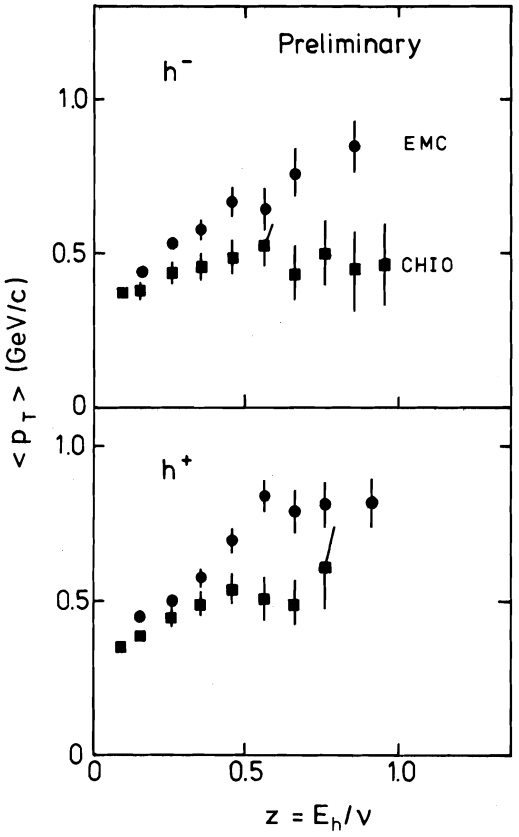

Fig. 12 Seagull effect for negative (h^-) and positive hadrons (h^+). The circles correspond to data from this experiment with $Q^2 > 5$ $(GeV/c)^2$ and $W^2 > 100$ GeV^2. The squares correspond to CHIO data with $Q^2 > 0{,}3$ $(GeV/c)^2$, $W^2 > 100$ GeV^2 and $\omega > 40$.

In the naive quark parton model the quarks have no transverse momenta. In the more fashionable quark models with perturbative QCD extensions the quark gluon coupling induces a transverse momentum $p_{T,QCD}$ [20]. In addition the struck quark may have a primordial transverse momentum $p_{T,frag}$ by the fragmentation of the quark[21].
The average p_T^2 of the observable hadrons therefore contains three contributions:

$$\langle p_T^2 \rangle = (\langle p_{T,prim}^2 \rangle + \langle p_{T,QCD}^2 \rangle)\, z^2 + \langle p_{T,frag}^2 \rangle$$

The factor z^2 is due to the fact, that only the fraction z of the struck quark momentum is transferred to the hadrons. As we have seen in Fig. 12 there is indeed a clear rise of p_T with z.
QCD predicts[22-24] a Q^2 dependence for the QCD contribution: the mean value $\langle p_{T,QCD}^2 \rangle$ should increase with Q^2:

$$\langle p_{T,QCD}^2 \rangle \propto Q^2/\ln\,(Q^2/\Lambda^2)$$

The other contributions should not depend on Q^2. Fig. 13 shows the Q^2 dependence of $\langle p_T^2 \rangle$ as measured by muon scattering and neutrino scattering. It is clear that the comparison between the different experiments is difficult since the experimental acceptances are widely different.

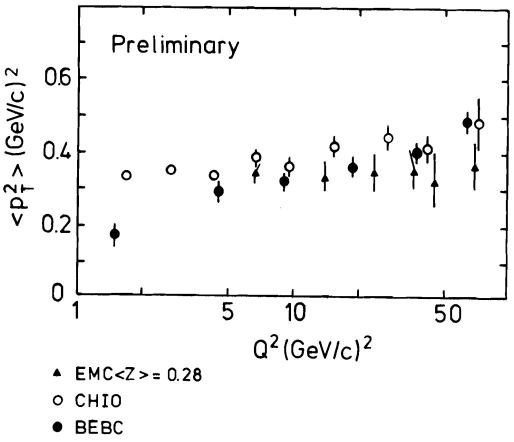

Fig. 13 Dependence of the mean value of the square of the hadron transverse momentum $\langle p_T^2 \rangle$ on Q^2 for muon experiments (EMC and CHIO) compared to neutrino results (BEBC).

But all experiments seem to agree that if there is any Q^2 dependence at all it must be very small. It is compatible with the slow variation predicted by QCD.

However a stronger dependence on W is predicted by the QCD models[25,26]. The QCD contribution should rise proportional to W^2:

$$\langle p_{T,QCD} \rangle \propto W^2/\ln(Q^2/\Lambda^2).$$

In Fig. 14 the $\langle p_T \rangle$ distribution as measured by muon scattering, neutrino scattering and suitably corrected[27] e^+e^- experiments show some weak linear increase with W^2.

Muon scatteting experiments have the advantage of fixing p_T by the kinematics of the incoming virtual photon.

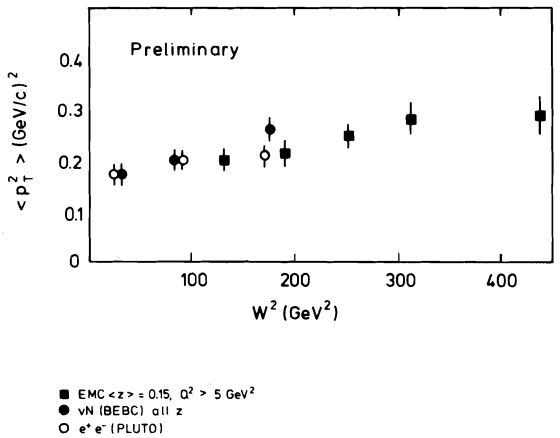

Fig. 14 Dependence of $\langle p_T^2 \rangle$ on W^2 for muon nucleon scattering (EMC data), neutrino nucleon scattering (BEBC data) and electron positron scattering (PLUTO data).

Neutrino experiments and electron positron scattering experiments have difficulties in fixing the current direction. In addition the strong dependence of the p_T distributions on the mean value of <z> accepted in the experiment as shown in fig. 15 prevents a more quantitative comparison between the different experiments.

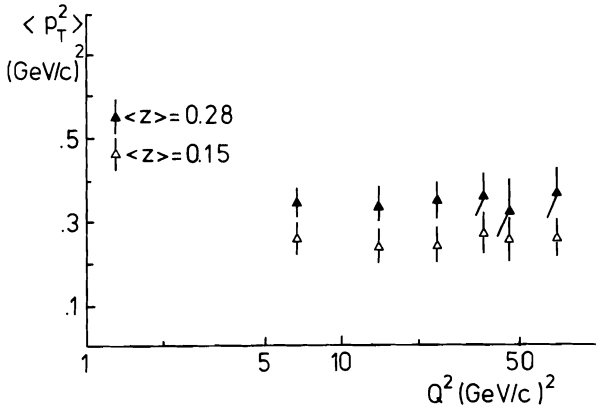

Fig. 15 Dependence of the $<p_T^2>$ distribution measured in this experiment on the mean value of z.

4.) Heavy Target Data

4.a) Structure Functions

Data on muon scattering on iron nuclei have been taken at 280 GeV incoming muon energy, for about 10^{11} muons hitting the target and at 250 GeV for about 5×10^{11} muons in total. The data presented to this conference correspond to 15% of the 280 GeV data. Data taking at 120 GeV with 10^{11} muons is foreseen for 1979.

Fig. 16 contains a schematic view of the iron scintillator sandwich counter, called STAC (Sampling Total Absorption Counter). 2.56m of iron are used as a target in the muon beam.

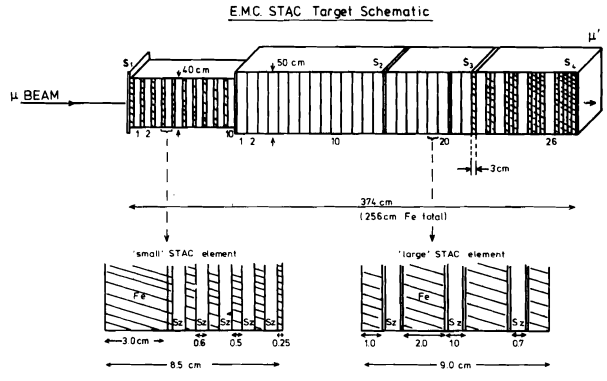

Fig. 16 STAC target (Sampling Total Absorption Counter).

Intersections of scintillator readout by 36 photomultipliers allow localization of the distribution of hadronic and electromagnetic showers in the target, if an interaction took place, and to measure the total energy deposit E with an energy resolution:

$$\frac{\Delta E}{E} = \frac{0,4}{\sqrt{E}} \text{ , with E in GeV.}$$

With the aid of this target the dependence of the structure function F_2 per nucleon on x and Q^2 as shown in fig. 17, has been measured. The physical interpretation of the structure function allows a direct comparison with the F_2 structure function as determined in neutrino nucleon scattering.

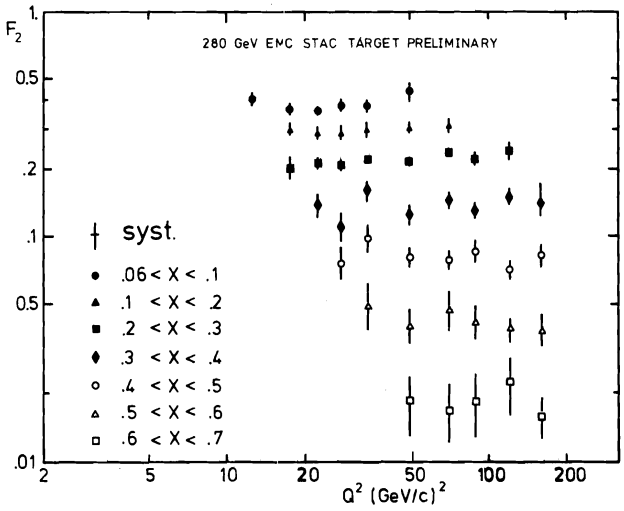

Fig. 17 - Structure function F_2 per nucleon measured by muon scattering on iron nuclei.

Considering the fractional charges of the quarks contributing to neutrino nucleon and muon nucleon scattering and assuming isospin invariance for the quarks, the ratio of the F_2 structure functions measured in the respective experiments should be 5/18. Fig. 18a and 18b therefore show a comparison of the structure function F_2 as measured in neutrino experiments[28] multiplied by this factor, to the EMC heavy target data for different ranges of x. Due to the still high systematic uncertainty in our data the agreement between neutrino and muon scattering experiments is very good, reflecting the success of the naive quark model with non-integral charges.

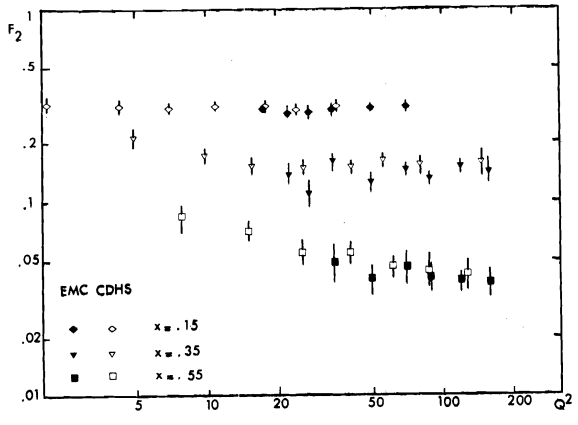

a)

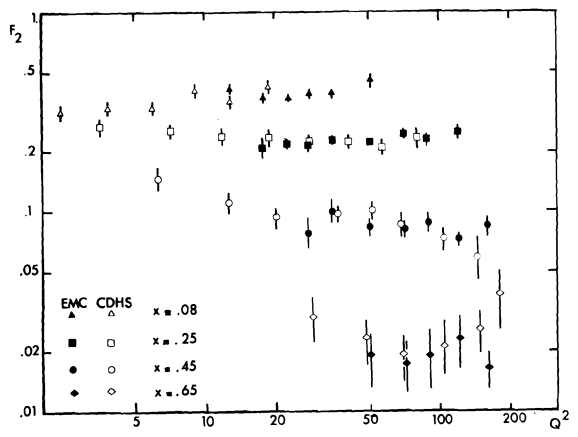

b)

Fig. 18 a) and b) Comparison of F_2 as determined by muon (EMC) and neutrino scattering (CDHS) on iron nuclei for different x ranges.

The observation of an important step in the structure function at a center of mass energy squared of 80 GeV^2 has been reported in a recent publication[29] and interpreted as a possible colour threshold[30]. As indicated in fig. 19 our subset of data plotted against W^2 does not show such a step, in contradiction to this experiment.

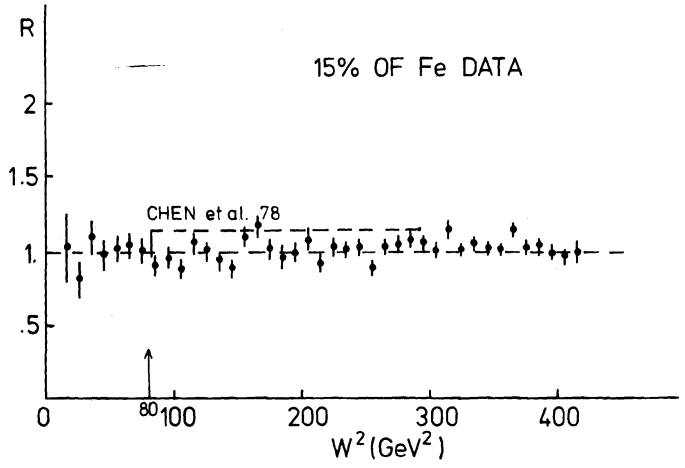

Fig. 19 Ratio R of the measured value of F_2 to the prediction of QCD calculations versus W^2. No indication for a step at 80 GeV^2, as reported in ref. 29 and indicated by a hatched line in the figure, is visible in the data.

Some data at 250 GeV muon energy have also been analysed improving essentially the statistical error of the 280 GeV data shown in fig. 19.

b.) Multimuon Data. Muon induced multimuon production is an interesting way to study associated charm production as well as the virtual photoproduction of bound $c\bar{c}$ states. The gluon distribution inside the nucleon can thus be investigated and other heavier quarks may show up in multimuon events.

Besides these especially interesting multimuon processes there are more conventional processes leading to multimuon production. Electromagnetic interactions produce muon pairs in two different ways exactly calculable by QED: bremsstrahlung[31-33] from the interacting particles, the muon and the target particles, and Bethe-Heitler production[34,35]. The corresponding timelike (Fig. 20a,b) and spacelike (Fig. 20c) graphs are shown in Fig. 20.

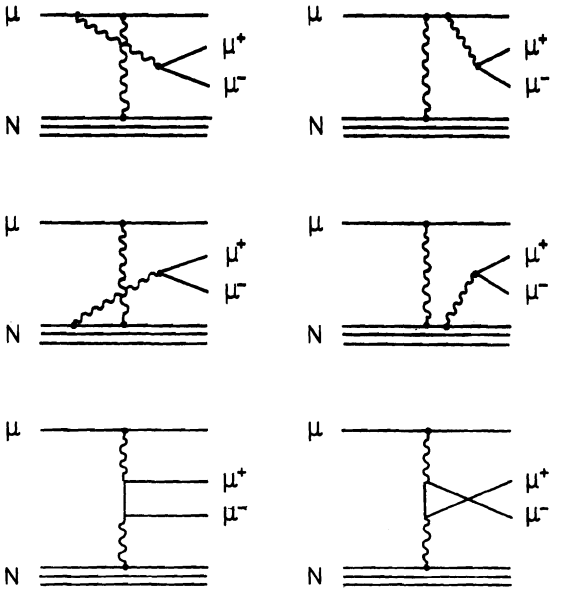

Fig. 20 Feynman diagrams for electromagnetic muon pair production: a) muon bremsstrahlung, b) target bremsstrahlung c)Bethe-Heitler process.

If the virtual photon interacts with a quark, a muon pair may be produced by deep inelastic Compton scattering off the quark. Pion and kaon production and their subsequent decay may also produce multimuon events as described by parton models[36-38].

Especially interesting is the QCD process of Bethe-Heitler $c\bar{c}$ and $b\bar{b}$ heavy quark production by photon-gluon fusion as recently discussed by Glück and Reya[39] and by Barger et al.[35]. The corresponding Feynman diagrams are shown in Fig. 21 for the production of $q\bar{q}$ bound states.

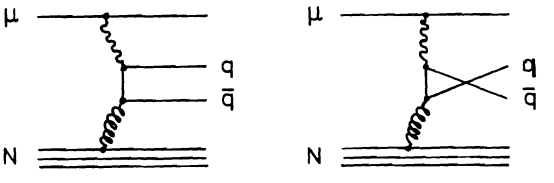

Fig. 21 $q\bar{q}$ production by photon gluon fusion. The heavy quarks can decay producing muons or muon pairs.

An important contribution to dimuon events is expected from D meson production with subsequent muonic decays. In this case neutrinos will carry away reaction energy, so that dimuon events with missing energy can be considered as a hint of free flavour production. Heavy lepton pair production like for instance $\tau^+\tau^-$ pair production is predicted to be unimportant[40-41] compared to charm production.

The heavy STAC target is well suited to search for processes producing multimuon final states. The first results have been reported in March 79 at Erice[42]. Momenta and angles of the outgoing muons were measured in the forward spectrometer. The energy balance between incident and outgoing particles could then be compared to the hadronic or electromagnetic shower energy measured in the STAC. About 10,000 $\mu^+\mu^+\mu^-$ events were obtained at 280 GeV/c beam momentum. The scattered muon was normally the higher momentum positive particle. The mass spectrum of the remaining muon pair is given in Fig. 22. J/ψ production is clearly visible.

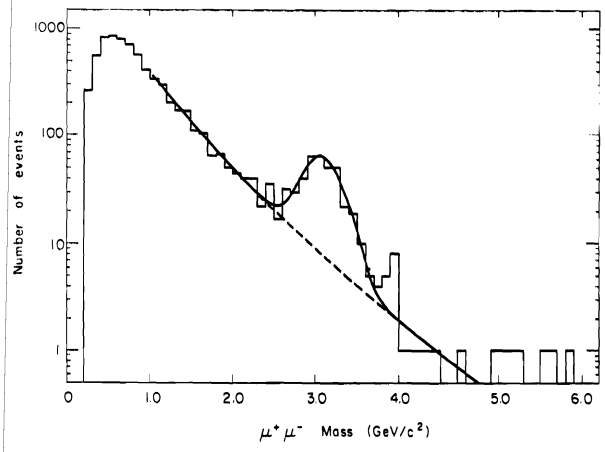

Fig. 22 - Dimuon mass spectrum with the J/ψ signal. The fit sshown is a gaussian plus a smooth background.

A fit to this distribution gave a mass resolution $\sigma = 0.22$ GeV/c^2 at the J/ψ mass in agreement with the calculated resolution.

The energy deposited in the STAC target by the events in the J/ψ mass region allowed a separation of elastically produced J/ψ events (energy deposit <5 GeV) from the inelastic events, which were about half of the events in this mass region. The vector meson dominance model treats the photon as being converted into a vector meson which then scatters elastically from the target. The Q^2 dependence is in this case determined by the vector meson propagator. This mechanism is supported by the Q^2 dependence of the data shown in Fig. 23.

A fit to this experimental distribution gave good agreement using the form $C(1+Q^2/M^2)^{-2}$ with C and M as free parameters. The best fit was obtained with $M = 2.45^{+0.37}_{-0.33}$ GeV showing the importance of the higher mass scale in the propagator.

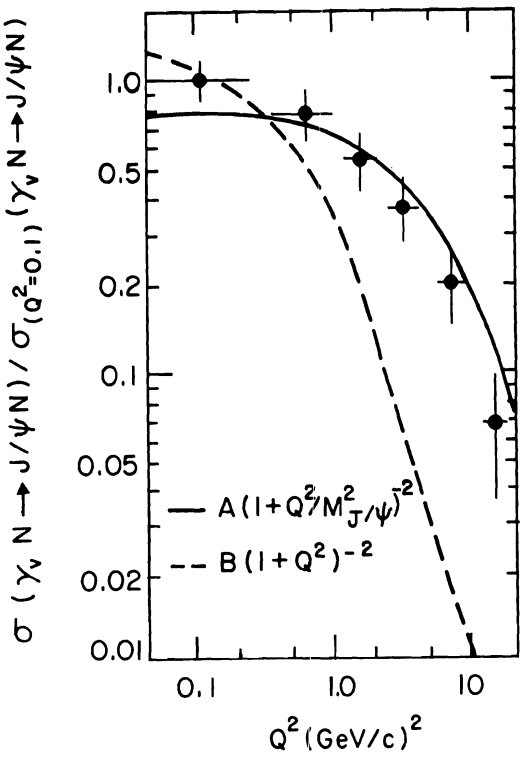

Fig. 23 Q^2 dependence of elastic J/Ψ production. The curves are best fits for VDM predictions with a propagator mass equal to 1 GeV (dotted line) and to the J/Ψ mass (solid line).

Fig. 24 gives the distribution of the events as a function of the variable $t' = t - t_{min}$. Coherent and incoherent scattering of virtual photons is visible.

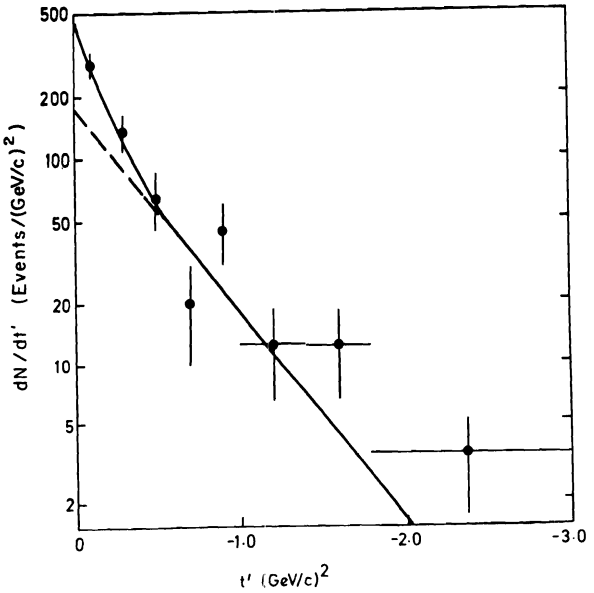

Fig. 24 t-distribution of elastic J/Ψ events compared to a parametrisation including coherent and incoherent production.

The slope parameter of the coherent contribution was not resolved due to the experimental resolution and was assumed to be a = 135 $(GeV)^{-2}$. The slope parameter b of the incoherent scattering was measured to be b = 2.31±30 $(GeV/c)^{-2}$. The Q^2 and t dependence have been used to calculate $d\sigma/dt$ at $Q^2 = 0$ and $t = 0$ for J/Ψ production. The result is shown in fig. 25 a as a function of ν. The elastic J/Ψ production data are consistent with a constant cross section of 52±5 nb/$(GeV/c)^2$.

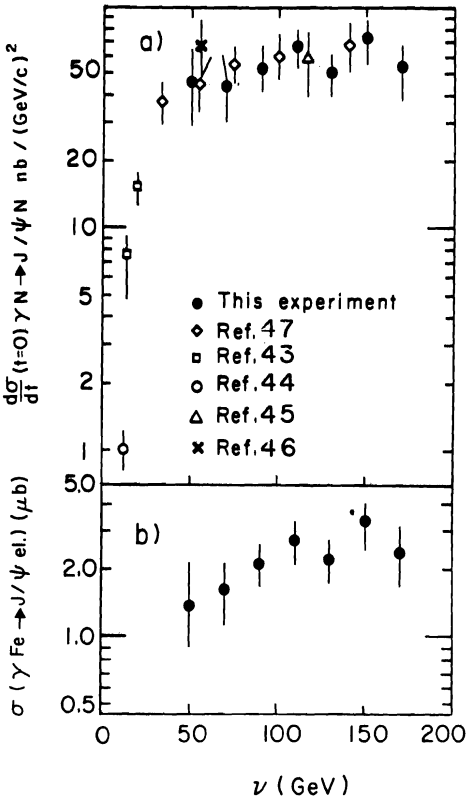

Fig. 25 Elastic J/Ψ photoproduction cross sections as a function of the photon energy ν: a) differential cross section, b) total cross section on iron.

The data are compared with photoproduction data[43-46] and recent muoproduction data[47]. Fig.25 b contains the elastic photoproduction cross section on iron as a function of ν. The inelastically produced J/Ψ events are still being studied.

The existence of genuine dimuon events with missing energy E_{miss} in the STAC target defined as

$$E_{miss} = E_{beam} - E_{\mu 1} - E_{\mu 2} - E_{STAC}$$

has been established. Fig. 26 shows the missing energy distributions of raw like sign and unlike sign dimuon events. On average there is a missing energy of about 20 GeV. These events are attributed to charm production.

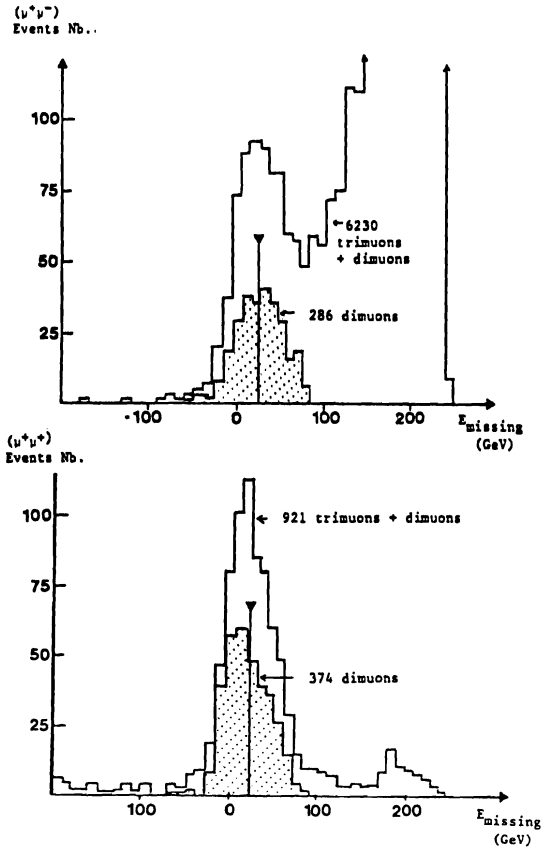

Fig. 26 - The dimuon sample missing energy - defined as $E_{missing} = E_{beam} - E_{\mu 1} - E_{\mu 2} - E_{target}$. The upper line is the sample before removing trimuons, the dashed area contains the dimuons left after cuts. The vertical line corresponds to 20 GeV mean missing energy in the dimuon sample.

Detailed background studies have still to be performed before a charm production cross section can be extracted from these data. Several events with more than 3 final state muons have been seen in the experiment and are being analysed.

5.) Future Experiments[48]

The next change of the experimental setup as shown in fig. 5 is the addition of a 450 channel lead glass detector in the forward direction to study direct photon and neutral hadron production. The second essential change will be the use of a polarized proton target to determine the spin dependent structure functions. Measurements with this target will start in March 1980.

In a further step the angular acceptance of the Forward Spectrometer will be increased to about ±60° by the addition of a Vertex Detector System as shown in fig. 27.

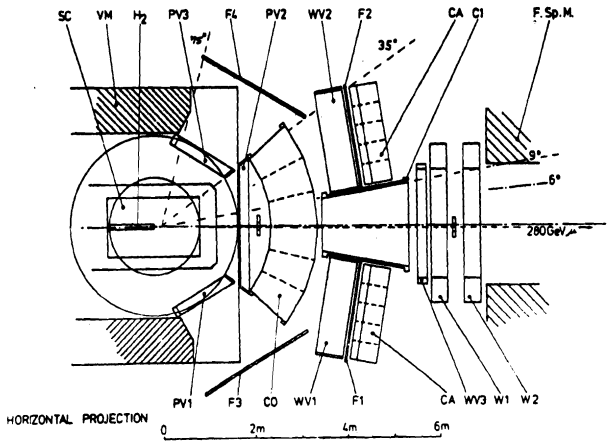

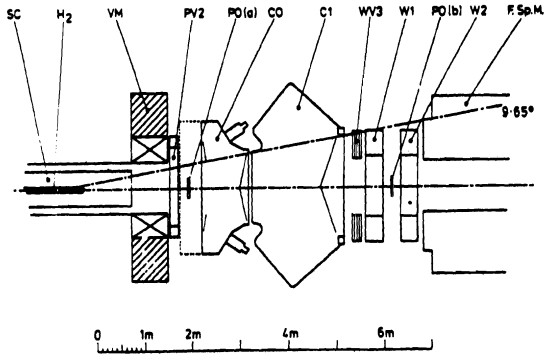

Fig. 27 Vertex detector system SC = streamer chamber, VM = vertex magnet, H_2 = hydrogen target, PV = proportional chambers, F = scintillation counter hodoscopes, WV = drift tube systems, C = Cerenkov counters).

A streamer chamber in a c-shaped vertex magnet will be used in connection with additional detectors to measure particle production. This system will essentially improve the study of complete final states in deep inelastic muon nucleon scattering. The study of heavy quark quantum numbers as well as the test of QCD predictions for the structure of final states makes the vertex system an additional interesting part of the EMC muon nucleon scattering experiment.

Acknowledgements

The author wishes to thank the Organizing Committee of this conference, Chairman J. Peoples, the Fermi National Accelerator Laboratory for their kind hospitality, and the scientific secretary D. Winn for his support. He is also very grateful to the secretaries A. Mazzari and C. Wagner. Without their admirable help in preparing the figures and typing the manuscript this paper would have never been completed.

References

1.) L.N. Hand, Phys. Rev. 129, 1834 (1963)

2.) E.D. Bloom et al., Phys. Rev. Lett. 23, 930(1969); M. Breidenbach et al., Phys. Rev. Lett. 23, 935(1969)

3.) S.D. Drell and J.D. Walecka, Ann. Phys. 28, 18(1964)

4.) R.P. Feynman, Photon Hadron Interaction, Benjamin, New York 1972

5.) G. Miller et al., Phys. Rev. D5, 528 (1972)

6.) J.D. Bjorken, Phys. Rev. 179, 1547 (1969)

7.) Y. Watanabee et al., Phys. Rev. Letters 35, 898 (1975); C. Chang et all, Phys. Rev. Letters 35, 901 (1975)

8.) R. Taylor, Proc. Internat. Symposium on Lepton and Photon Interaction at High Energies, Stanford 1975, p. 679

9.) C.H. Llewellyn Smith, Proc. Internat. Symposium on Lepton and Photon Interactions at High Energies, Stanford 1975, p. 709

10.) A. de Rujula, H. Georgi and H.D. Politzer, Ann. Phys. 103, 315 (1977)

11.) J. Kogut and L. Susskind, Phys. Rev. D9, 3391 (1974)

12.) G. Altarelli and G. Parisi, Nucl. Phys. B 126, 298 (1977)

13.) F.E. Close, CERN preprint Ref. TH. 2594-CERN (1978)

14.) European Muon Collaboration, "Proposed Experiments and Equipment for a Programme of Muon Physics at the SPS", CERN/SPSC/74-78/P. 18 (1974)

15.) W. Flauger, Nucl. Instr. and Methods 165, 119 (1979)

16.) H.E. Stier, paper presented at the "Seminar on probing Hadrons with Leptons", Erice, March 1979, proceedings to be published

17.) V. Korbel, paper presented at the "XIVth Rencontre de Moriand", Proceedings 1979

18.) P. Payre, paper presented at the "XIVthe Rencontre de Moriand", Proceedings 1979

19.) A.J. Buras and B.G.F. Gaemers, Nucl. Phys. B 132, 249 (1978); A.J. Buras, FERMILAB-Pub. 79/17-THY

20.) A. Mendez, Nucl. Phys. B 145, 199 (1978)

21.) M. Glück, E. Reya, Nucl. Phys. B 145, 24 (1978)

22.) H.D. Politzer, Phys. Rep. 14 C (1974)

23.) G. Altarelli, G. Martinelli, Phys. Letters 76 B, 89 (1978)

24.) A. Mendez, A. Raychaudhuri, V.J. Stenger, Nucl. Phys. B 148, 499 (1979)

25.) P. Mazzanti, R. Odorico, V. Roberto, Phys. Letters 81 B, 219 (1979)

26.) G. Altarelli, Proceedings of the "XIIIthe Rencontre de Moriand", Vol. 2, 395 (1978)

27.) R. Odorico, preprint 1979

28.) J.G.H. de Groot et al., Phys. Letters 82 B, 456 (1979) and Z. Physik C1, 143 (1979)

29.) R.C. Ball et al., Phys. Rev. Letters 42, 866 (1979)

30.) E. Lehman, Phys. Rev. Letters 42, 869 (1979)

31.) K. J. Evans, Nucl. Phys. B 75, 171 (1974)

32.) V. Ganapathi and J. Smith, I TP-SB-78-45

33.) Y.S. Tsai, Rev. Mod. Phys. 46, 815 (1974)

34.) S. Brodsky and SU Ting, Phys. Rev. 145, 1018 (1966)

35.) V. Barger, W.Y. Keung, R.J.N. Phillips, Phys. Rev. D 20, 630 (1979)

36.) R.D. Field, R.P. Feynman, Nucl. Phys. B 136, 1 (1978)

37.) T. Hansl et al., Nucl. Phys. B 142, 381 (1978)

38.) V. Barger et al., Phys. Rev. D 18, 2308 (1978)

39.) M. Glück and E. Reya, Phys. Letters 79 B , 453 (1978) and Phys. Letters 83 B, 98 (1979)

40.) Y.S. Tsai, SLAC-PUB-2356 (1979)

41.) P. Kessler, Nuovo Cimento 53, 809 (1960)

42.) J.J. Aubert, paper presented at the "Seminar on Probing Hadrons with Leptons", Erice, March 1979, proceedings to be published

43.) U.Camerini et.al., Phys. Rev. Lett. 35, 483 (1975).

44.) B.Gittelman et.al., Phys. Rev. Lett. 36, 1616 (1975).

45.) B.Knapp et. al., Phys. Rev. Lett. 34, 1040 (1975).

46.) T.Nash et.al., Phys. Rev. Lett. 36, 1233 (1976).

47.) A.R.Clark et. al., Phys. Rev. Letters 43, 187 (1979).

48). European Muon Collaboration, CERN/SPSC/77-113/ P.18/ Add. 1 (1977) and CERN/SPSC/79-17/P.18/ Add. 2 (1979).